6th International Conference on Multiphase Flow,
ICMF 2007, Leipzig, Germany, July 9 – 13, 2007

Effect of the vapor phase on the near-wall velocity field in subcooled boiling flow

Franz Ramstorfer[1], Helfried Steiner[2] and Günter Brenn[2]

[1]The Virtual Vehicle Competence Center GmbH
Inffeldgasse 21A, Graz, 8010, Austria
franz.ramstorfer@virtuellesfahrzeug.at

[2]Graz University of Technology, Institute of Fluid Mechanics and Heat Transfer
Inffeldgasse 25F, Graz, 8010, Austria
steiner@fluidmech.tu-graz.ac.at

Keywords: subcooled boiling flow, turbulent boundary layer, modified law of the wall

Abstract

In subcooled boiling flow, the heat transfer process is mainly constituted by the exchange of latent heat associated with evaporation and condensation, as well as the bubble-induced convective transport. Most state-of-the-art models for the total wall heat flux in boiling flow account for the latter effect, generally termed micro convection, by introducing an empirically determined enhancement factor of the macroscopic convection of the liquid bulk flow. The present work proposes a less heuristic approach, which more closely reflects the dynamic effects of the vapor bubbles on the near-wall liquid flow field.
Performing subcooled boiling flow experiments, the velocity field inside the bubble-laden superheated wall layer was investigated. LDA measurements of the liquid velocity field showed that the vapor bubbles generally lead to a significant reduction of the streamwise mean velocity of the liquid. For increasing wall heat fluxes the decelerating effect of the vapor bubbles becomes stronger, which is indicated by the parallel shift of the velocity profiles to lower values. The measurements also clearly demonstrated the significantly enhanced turbulence in the near-wall region caused by the micro convective effects of the bubbles. Since the experimentally observed characteristics of the liquid velocity field turned out to be very similar to turbulent flows along rough surfaces, it is proposed to model the near-wall effect of the bubbles on the liquid flow analogously to the effect of a surface roughness. The modeled roughness heights were shown to correlate very well with the experimentally observed bubble diameters at the instant of bubble detachment from the heated surface. Incorporating the proposed approach as a dynamic boundary condition into a well-established mechanistic flow boiling model makes it possible to reflect adequately the contribution of the micro convection to the total wall heat transfer. The limits of this approach are examined based on a dimensional analysis. In a nomogram of the Jakob number versus the Froude number, a buoyancy-dependent regime can be separated from a buoyancy-independent regime. Within the limits of the buoyancy-independent regime, the roughness-based concept is proven to reflect very well the main characteristics of the near-wall liquid flow for a wide range of experimental conditions.

Introduction

A reliable mathematical description of the heat flux across a heated surface as a function of the local wall superheat in subcooled flow boiling is becoming increasingly important for the design of highly efficient liquid cooling systems. A large number of wall heat flux models have been proposed in the past and are still further developed (Chen (1963), Kutateladze (1963), Shah (1977), Liu & Winterton (1991), Steiner & Taborek (1992), Wenzel & Müller-Steinhagen (1994), Kandlikar (1998), Campbell *et al.* (2002), Steiner *et al.* (2005)). Due to the high complexity of the problem involving a great variety of thermophysical effects, which are often hard or even impossible to measure, no rigorous analytical description of the nucleate boiling process has been derived yet. Therefore, most state-of-the-art models rely on a good deal of empiricism in terms of adjustable model parameters.
A certain class of models assumes the total wall heat flux q_w as a single-phase convective base heat flux, which is enhanced by a factor beyond the onset of boiling. Models of this type, as proposed by, e.g., Shah (1977) and Kandlikar (1998), write the total wall heat flux q_w generally as the product

$$q_w = q_{conv,1ph}\,\psi_{2ph}\,, \qquad (1)$$

where $q_{conv,1ph}$ represents the single-phase convective heat flux, which is multiplied by an enhancement factor ψ_{2ph}. The enhancement factor is in general modeled as a function of the Boiling number Bo, such that

$$\psi_{2ph} = \psi_{2ph}(\mathrm{Bo}) \text{ with } \mathrm{Bo} = \frac{q_w}{\dot{m}\, h_{fg}} . \qquad (2)$$

The boiling number describes the ratio of the total wall heat flux q_w to the heat flux necessary to evaporate completely the mass flux $\dot{m}$ of the bulk liquid. The essential shortcoming of this class of models arises when approaching the limit of pool boiling, since the Boiling number goes by definition to infinity for vanishing mass flux $\dot{m}$.

An alternative approach to the multiplicative concept of Eq. (1) is represented by the superposition models. This widely used concept, which was introduced by Chen (1963), assumes the total wall heat flux to be additively composed of a macroscopic, convective component and a microscopic, nucleate boiling component. Accordingly, the super-imposed total wall heat flux is written as

$$q_w = q_{conv,1ph}\, F_{2ph} + q_{nb}\, S . \qquad (3)$$

This linear decomposition is attractive for two reasons. First, it offers much freedom in choosing most adequate submodels for each component. Secondly, it provides the correct asymptotics at the transition to the non-boiling regime, where the nucleate boiling component q_{nb} becomes zero and only the macroscopic, single-phase convection $q_{conv,1ph}$ remains. The macroscopic component is mostly obtained from typical textbook correlations for forced convective channel flows, such as the Dittus-Boelter correlation. The microscopic contribution is generally computed using well-established pool boiling models, such as those proposed by Rohsenow (1952), Forster & Zuber (1955), Cooper (1984) or Gorenflo (1988). The factor F_{2ph} in Eq. (3) represents the enhancement of the single-phase convective component by the bubble agitation. Based on experimental data, Chen (1963) correlated F_{2ph} with the inverse of the Martinelli number X_{tt}, such that

$$F_{2ph} = F_{2ph}(X_{tt}) \text{ with } X_{tt} = \left(\frac{1-x_v}{x_v}\right)^{0.9} \left(\frac{\mu_l}{\mu_v}\right)^{0.1} \left(\frac{\rho_v}{\rho_l}\right)^{0.5} , \qquad (4)$$

where x_v denotes the mass fraction of the vapor.

Since the boiling activity can be strongly suppressed by the flow of the bulk liquid, especially at lower superheats $\Delta T_w = T_w - T_{sat}$, the nucleate boiling contribution q_{nb} turns out to be effectively smaller than the pool boiling heat flux. For this reason, Chen (1963) introduced a flow-induced suppression factor S. The suppression factor S decreases from S = 1 to S = 0 for increasing flow Reynolds number. Chen's concept was adopted by many authors using different submodels for the pool boiling heat flux and various correlations for the suppression factor S (Liu & Winterton (1991), Wenzel & Müller-Steinhagen (1994), Campbell et al. (2002), Steiner et al. (2005)).

Similarly to Chen's ansatz given by Eq. (4) most mechanistic models correlate the enhancement factor F_{2ph} as a function of the mass fraction of the vapor. This imposes a serious practical difficulty in the case of subcooled boiling flow. In this regime the vapor bubbles exist only in a very confined superheated layer close to the wall, which makes it difficult to measure the mass fraction of the vapor as a reliable input parameter to these models. For this reason many authors simply neglect the effect of the bubbles on the convection by setting the two-phase convection enhancement factor to unity, $F_{2ph} = 1$. On the other hand, flow boiling experiments such as those carried out by Maurus (2003) demonstrated very clearly a significant influence of the bubbles on the liquid flow field, also in the case of subcooled boiling flow. In his experimental study, Maurus investigated the mean velocity profiles for varying heat flux, flow Reynolds number, and subcooling $\Delta T_{sub} = T_{sat} - T_b$ using a PIV measurement technique.

Roy *et al.* (1997, 2002) studied subcooled boiling flow of R-113 in a vertical annular channel, where only the inner wall was heated. For their measurements in the two-phase boundary layer they used simultaneously a two-component laser-Doppler anemometer for the liquid velocity field, a cold wire for the temperature field, and a dual-sensor fiberoptic probe for the vapor fraction and vapor axial velocity. Based on their measurements they proposed a standard logarithmic wall function with somewhat modified constants for use as boundary condition for the liquid velocity in a two-fluid simulation.

The present work starts out from a series of subcooled boiling flow experiments, which are performed with varying wall heat flux and flow Reynolds number. In our experiments, the near-wall velocity field is closely investigated using a laser-Doppler anemometer, which allows for the measurement of the mean velocity profiles as well as the profiles of the turbulent fluctuations of the liquid phase. Based on the obtained experimental findings, a wall model is proposed, which reflects adequately the experimentally observed features of the near-wall flow for use in a single-fluid modeling of the total wall heat flux.

Nomenclature

Bo	Boiling number (–)
c	specific heat capacity of the liquid (J/kg K)
C	integration constant (–)
C_{kr}	roughness constant (–)
C_{krc}	roughness constant (–)
C_{sf}	parameter (–)
d	bubble diameter (m)
D_h	hydraulic diameter (m)
Ec	Eckert number (–)
F_{2ph}	enhancement factor (–)
Fr	Froude number (–)
g	gravitational acceleration (m/s²)
h_{fg}	specific latent heat of evaporation (J/kg)
Ja	Jakob number (–)
k_r	physical roughness height (m)
$\tilde{k}_r$	modeled roughness height (m)
m	model constant (–)
$\dot{m}$	mass flux (kg/m²s)
p	pressure (bar)
q	heat flux (W/m²)
Re	Reynolds number (–)
Re_b	bubble Reynolds number (–)
S	suppression factor (–)
T_{sat}	saturation temperature (K)

ΔT_{sub}	$= T_{sat} - T_b$ subcooling (K)
ΔT_w	$= T_w - T_{sat}$ wall superheat (K)
u	velocity in the streamwise direction (m/s)
u_τ	$= \sqrt{\tau_w / \rho_l}$ wall friction velocity (m/s)
v	velocity in the wall-normal direction (m/s)
x	coordinate in the streamwise direction (mm)
x_v	mass fraction of vapor (–)
X_{tt}	Martinelli number (–)
y	distance from the heated wall (m)

Greek letters

γ	model parameter (–)
δ	model parameter (–)
Δ	difference
ε	convergence criterion (–)
$\overline{\varepsilon}$	turbulent dissipation rate (m^2/s^3)
ζ	model parameter (–)
η	model parameter (–)
κ	von Kármán constant (–)
λ_f	friction coefficient (–)
μ	dynamic viscosity of the liquid (kg/ms)
ν	kinematic viscosity of the liquid (m^2/s)
ρ	density (kg/m^3)
σ	surface tension (N/m)
τ	shear stress (N/m^2)
τ_{drag}	bubble relaxation time (s)
τ_{flow}	turbulent flow time scale (s)
ψ_{2ph}	enhancement factor (–)

Subscripts

b	bulk
conv	convective
l	liquid
m	median
nb	nucleate boiling
rms	root mean square
v	vapor
w	wall
1ph	single-phase
2ph	two-phase

Superscripts

n	number of iteration step
+	quantities in wall units

Experimental Setup

The experimental facility, which is sketched schematically in Figure 1, basically consists of a closed loop channeling a forced convective flow driven by a pump. The working fluid passes through a heated test section, which is schematically shown in Figure 2. The bulk velocity, the bulk temperature of the liquid, and the operating pressure at the inlet of the section are controlled. In the present configuration, the bulk velocity may be varied within the range of $0.05 \text{ m/s} \le u_b \le 2.0 \text{ m/s}$, which corresponds to a range of flow Reynolds numbers between 5629 and 45030. The absolute operating pressure can be set within the range $1.0 \text{ bar} \le p \le 2.0 \text{ bar}$. The square-shaped cross section of the test section has the dimensions 36 x 36 mm^2. The heat transfer to the flowing liquid is provided by electrically heated coils located at the bottom of the aluminum heater from where the heat is conducted to the heater surface. The heater surface (grey shaded in Figure 2), which is the heated area of the test section, has a streamwise length of 65 mm and a width of 10 mm.

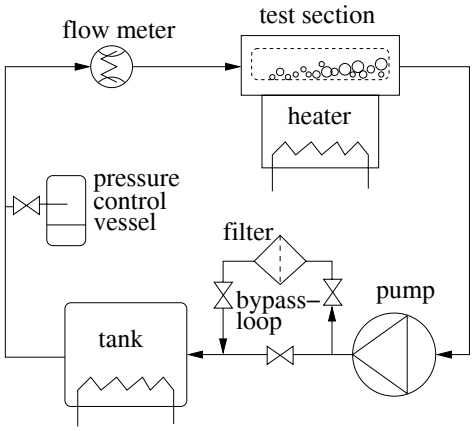

Figure 1: Schematic diagram of the subcooled boiling flow loop.

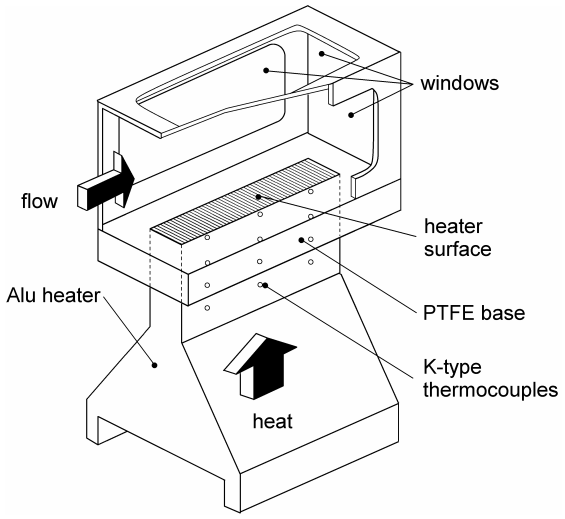

Figure 2: Test section of the experimental facility.

The wall temperature and the wall heat flux are determined based on Fourier's law of heat conduction using the temperatures measured with twelve K-type thermocouples appropriately distributed in the solid heater. The position of the individual thermocouples can be seen from Figure 2. The base plate of the test section, where the top of the aluminum heater is embedded, is made of PTFE. The very low thermal conductivity of PTFE should guarantee the lowest possible heat loss from the heater material to the surrounding structure. Due to thermal durability restrictions of the PTFE base plate, the maximum heater surface temperature was limited to $T_w = 160$ °C. Windows made of glass are embedded in the top as well as in the side walls of the test section to make the section optically accessible.
The size and motion of the bubbles were recorded using a high-speed camera. A 2D laser-Doppler anemometer from DANTEC was used for the liquid velocity measurements. Laser-Doppler anemometry has become a well-established

technique for local velocity measurements in transparent single-phase flows because of its high accuracy, good spatial and temporal resolution, and non-intrusive features. In general, the flow is seeded with tracer particles, which serve as scattering centers for the laser light. In the case of flow boiling experiments, no seeding particles may be added to the liquid, since they might affect the nucleate boiling process. While small, particle-like contaminations in the working liquid serve as scattering centers in the outer single-phase region, a sufficiently high signal rate is provided by the vapor bubbles in the two-phase region. Using the vapor bubbles as tracers for the liquid flow inherently assumes the slip between the bubbles and the liquid phase to be negligibly small. The validity of this assumption can be justified by comparing the bubble relaxation time based on the bubble drag force to the relevant turbulent flow time scale. The former is estimated following Mei *et al*. (1994)

$$\tau_{drag} = \frac{\rho_v d_m^2}{12\mu}\left\{1+\left[8/Re_b+1/2\left(1+3.315\,Re_b^{-0.5}\right)\right]^{-1}\right\}^{-1}, \quad (5)$$

where Re_b is the bubble Reynolds-number $Re_b = d_m u_b / \nu$ using the median bubble detachment diameter from the high-speed camera recordings as the length scale. The latter is estimated based on Kolmogorov's second similarity hypothesis, assuming that the bubble diameter lies well within the inertial subrange of the wavelength spectrum of turbulence, such that one may write

$$\tau_{flow} = \left(\frac{d_m^2}{\bar{\varepsilon}}\right)^{1/3}. \quad (6)$$

Here $\bar{\varepsilon}$ denotes the average dissipation rate of kinetic energy per unit mass. It is estimated in terms of the pressure loss of a turbulent channel flow, which reads

$$\bar{\varepsilon} = \frac{\Delta p}{\Delta x}\frac{u_b}{\rho} \quad \text{with} \quad \frac{\Delta p}{\Delta x} = \frac{\lambda_S}{D_h}\rho\frac{u_b^2}{2}. \quad (7)$$

Using the Blasius law for the wall friction coefficient, we have $\lambda_S = 0.316\,Re^{-0.25}$. The Reynolds number $Re = u_b D_h / \nu$ is based on the bulk flow quantities. In all considered cases the bubble relaxation time turned out to be about three orders of magnitude smaller than the turbulent flow time scale such that $\tau_{drag} / \tau_{flow} << 1$. This indicates clearly that the bubbles accurately follow the turbulent liquid motion and are therefore suitable as tracers for the LDA measurements.

The maximum total error relative to the measured heat flux is estimated as ±5 % in the convective regime and ±2 % in the nucleate boiling regime. The error in the measured surface temperatures is ±0.15 °C. The inductive flow meter measures the bulk velocity with a relative error of ±0.5 % of the displayed value.

Experimental Conditions and Results

In all our experiments, the working fluid was a mixture of ethylene glycol and water in a volumetric composition of 40/60 vol. %. The absolute system pressure p = 1.5 bar, as well as the subcooling $\Delta T_{sub} = T_{sat} - T_b = 22$ K were kept constant in all experiments. The wall heat flux q_w was varied between very low values and a maximum of about 500 kW/m², leading to a maximum wall superheat of about $\Delta T_w = T_w - T_{sat} = 40$ K. The bulk velocity of the working fluid was varied within the range of $0.1\ m/s \le u_b \le 0.8\ m/s$. The corresponding Reynolds number based on the bulk flow quantities ranges from 5629 to 45030.

The heat transfer conditions of all experimentally investigated cases can be seen from Figure 3, where the corresponding measured total wall heat flux q_w is plotted vs. the wall superheat ΔT_w.

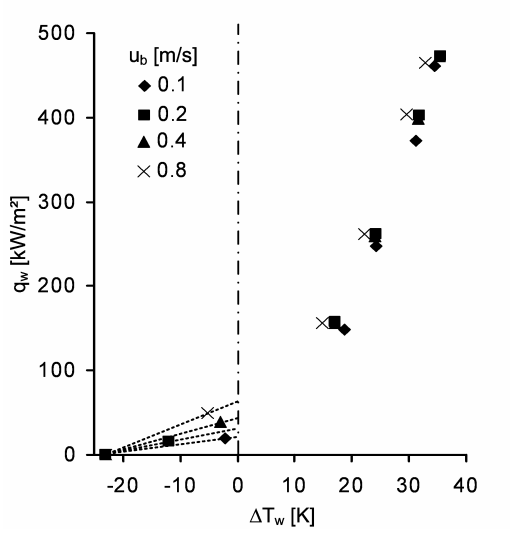

Figure 3: Measured total wall heat flux q_w vs. the wall superheat ΔT_w at different bulk velocities u_b. The dashed lines represent the single-phase macro-convection. The dash-dotted line denotes the saturation temperature ($\Delta T_w = 0$).

Most cases lie well inside the nucleate boiling region to the right of the saturation line $\Delta T_w = 0$. For each bulk velocity, at least one purely convective, non-boiling case, associated with $\Delta T_w < 0$, is investigated as well. The data point on the abscissa refers to the unheated reference cases without heat transfer to the liquid (denoted with $q_w = 0$) for use in the comparison with the bubble-laden, boiling cases in the discussion of the measured near-wall velocity profiles.

The results of the LDA measurements for all cases in Figure 3 are displayed in Figures 4 to 7. The mean values of the velocity components $\bar{u}$ and $\bar{v}$ in the streamwise and the wall-normal directions, respectively, as well as the rms-values of the corresponding fluctuations, u_{rms} and v_{rms}, are plotted against the wall-normal distance y. All displayed velocity profiles are scaled with the bulk velocity u_b. A comparison with the unheated bubble-free reference cases ($q_w = 0$) makes evident that the bubbles affect the flow considerably in the superheated near-wall layer.

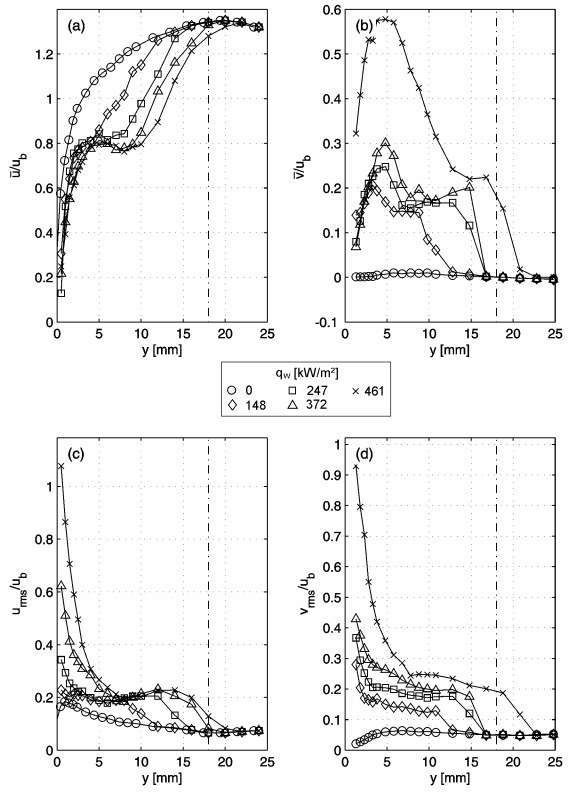

Figure 4: Results of the LDA measurements at the bulk velocity u_b = 0.1 m/s for varying heat flux q_w. The dash-dotted line marks the center of the test channel.

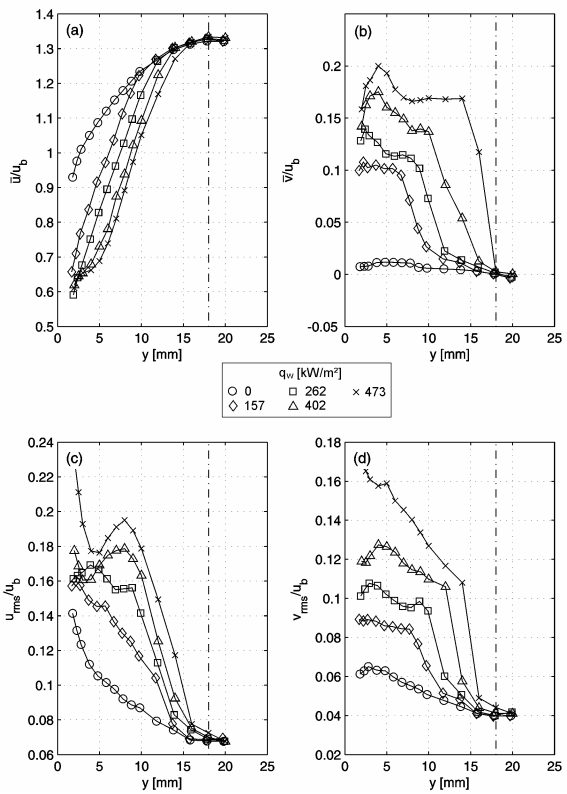

Figure 5: Results of the LDA measurements at the bulk velocity u_b = 0.2 m/s for varying heat flux q_w. The dash-dotted line marks the center of the test channel.

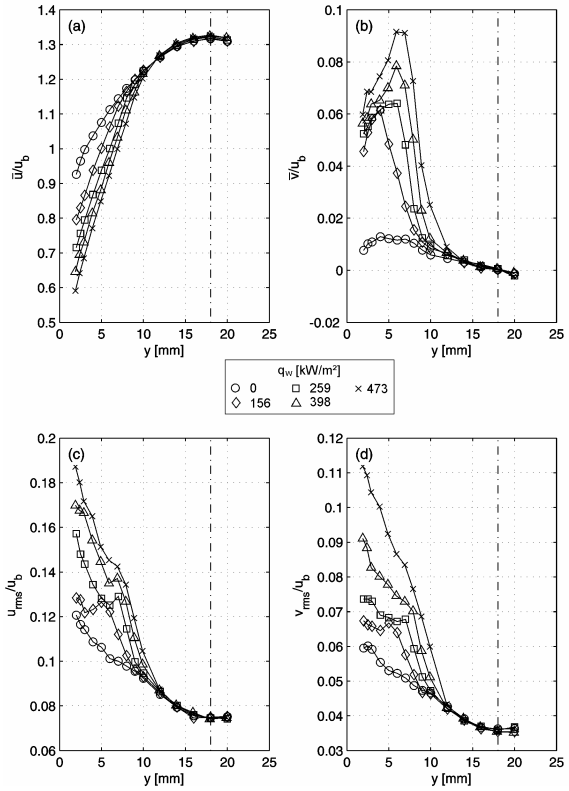

Figure 6: Results of the LDA measurements at the bulk velocity u_b = 0.4 m/s for varying heat flux q_w. The dash-dotted line marks the center of the test channel.

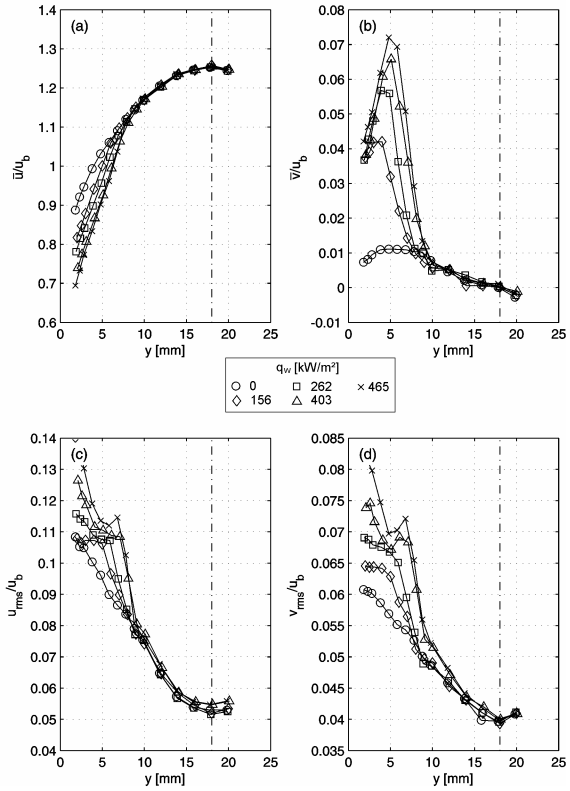

Figure 7: Results of the LDA measurements at the bulk velocity u_b = 0.8 m/s for varying heat flux q_w. The dash-dotted line marks the center of the test channel.

This influence becomes more pronounced with increasing boiling activity on the surface, as wall heat fluxes become higher. In the core flow region outside the superheated layer, the velocity profiles merge with the single-phase velocity of the non-boiling cases. Figures 4a to 7a show that in the two-phase region, the mean velocity $\overline{u}(y)$ in the streamwise direction is always significantly reduced against the non-boiling case. The presence of the vapor bubbles on the heated surface evidently generates an additional drag force on the mean flow. For continuity reasons the strongly retarded streamwise velocity is accompanied by a stronger displacement of liquid away from the wall, as indicated by the increased wall-normal component $\overline{v}(y)$ in Figures 4b to 6b. In the cases of very low bulk velocities ($u_b = 0.1$ m/s, $u_b = 0.2$ m/s) and high heat fluxes, the maximum of the mean wall-normal velocity component assumes the same order of magnitude as the streamwise component $\overline{u}(y)$, and the profiles for the streamwise component exhibit non-monotonous behavior (see Figures 4a and 5a). In this regime, the upper boundary of the bubble-laden layer shows a significant waviness, as seen on the photograph in Figure 8. The wavy shape of this boundary could be explained by the action of clockwise rotating vortical structures generated by the interaction between the rising bubbles and the relatively slow horizontal motion of the underlying liquid flow. This indicates that the buoyancy-induced vertical momentum is obviously of the same strength as the momentum in the streamwise direction. Accordingly, the values $\overline{v}/u_b$ are of order unity, as seen from Figures 4b and 5b.

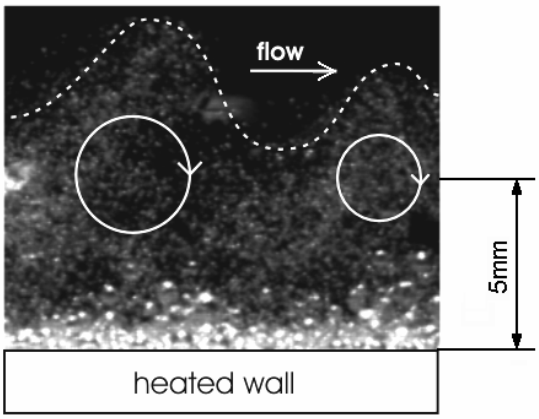

Figure 8: Photograph of the bubble-laden near-wall region at a bulk velocity of $u_b = 0.2$ m/s and a wall heat flux of $q_w = 402$ kW/m². The dashed line marks the upper boundary of the vortical layer. The circles denote clockwise rotating vortices.

As shown in Figures 4c and d to 7c and d, the presence of the bubbles causes a marked increase of the mean turbulent fluctuations in the streamwise and the wall-normal directions, $u_{rms}(y)$ and $v_{rms}(y)$, respectively, in the two-phase region of the flow. The observed increase of the turbulent velocity fluctuations in the near-wall region leads to enhanced momentum and heat transfer. As such, the bubble-induced convective mixing strongly contributes to the total heat flux achievable in subcooled boiling flow as compared to single-phase convection.

The impact of the bubbles on the flow field presumably depends strongly on the bubble size at the heated wall. Therefore, the bubble diameters at the instant of detachment from the heated surface were measured using high-speed camera recordings for the different boiling cases depicted in Figure 3. The median bubble diameters d_m observed in these experiments are shown in Figure 9. A higher wall heat flux leads to larger bubble sizes, as expected. On the other hand, the median bubble sizes decrease with increasing liquid flow velocity.

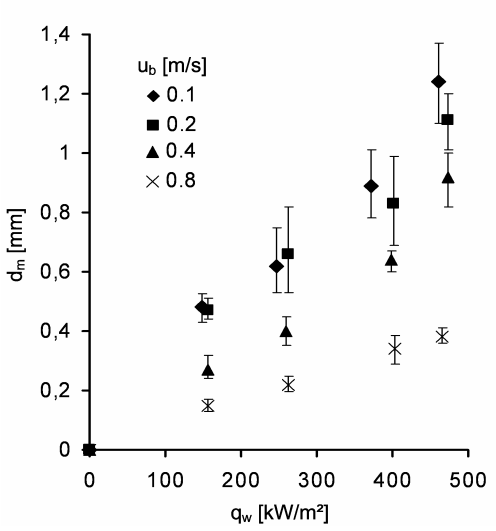

Figure 9: Measured bubble diameter d_m vs. the wall heat flux q_w at different bulk liquid velocities u_b. The rms fluctuations around the statistical median value are quantified by the "error" bars.

This illustrates the considerable impact of the liquid flow field on the bubble detachment process. Two major effects, a dynamical and a thermal one, can be distinguished here. First, higher liquid velocities are associated with stronger hydrodynamic forces, such as drag, shear lift forces, etc., which clearly affect the process of bubble growth and detachment from their nucleation sites. Secondly, the superheated thermal boundary layer becomes thinner as the liquid velocity increases. This conceivably limits the growth of the bubbles, since they cannot protrude into the subcooled outer layer, where the local temperature is by definition lower than the saturation temperature T_{sat}.

Modeling

Most of the models proposed for the liquid velocity field in bubble-laden boundary layer flows were developed for non-boiling flow, where the gas bubbles are injected through the porous channel walls. Typical representatives are the studies of Troshko & Hassan (2001) and Mikielewicz (2003). Troshko & Hassan (2001) proposed a model for the non-boiling case, which captures the bubble-induced increase of turbulence by adding a further term to the eddy viscosity. They modeled this bubble-induced contribution to the eddy viscosity as mainly depending on the void fraction of the gaseous phase. Mikielewicz (2003) incorporated the enhanced turbulence

associated with the presence of the bubbles by introducing an additional dissipation term. This additional dissipation is again determined as a function of the void fraction, and it further involves the terminal rise velocity of an upward moving bubble in a quiescent fluid as a velocity scale. Since both approaches, Troshko & Hassan (2001) and Mikielewicz (2003), essentially depend on the void fraction as a key input parameter, they can hardly be extended to the subcooled boiling flow case. In contrast to the non-boiling case, where the void fraction can be determined fairly accurately from the given gas injection through the porous walls, the void fraction in the flow boiling case results from the whole process of bubble nucleation, growth, detachment, and collapse. As such, being determined by the complex interaction of various sub-processes, its estimation based on the given thermophysical conditions in the near-wall region, such as wall superheat, subcooling, pressure, etc., is inevitably affected by much uncertainty. Moreover, since the bubbles collapse once they leave the superheated wall layer, the vapor phase exists only in a thin near-wall region. Dealing with a very thin, densely populated two-phase layer makes it almost impossible to obtain reliable experimental data for the void fraction, neither when using optical, nor with intrusive methods.

The difficulty in estimating and/or measuring a relevant void fraction in subcooled boiling flow with sufficient accuracy, needed as an essential input to the models, suggested to go for an alternative approach, which was originally proposed by Gabillet *et al.* (2002). They also investigated the non-boiling case in a horizontal channel flow configuration, where the bubbles were injected through the porous lower channel wall. They observed that the effect of the bubbles on the liquid flow was very similar to the effect of a surface roughness. Exploiting this similarity, they proposed to capture the influence of the bubbles on the liquid flow field using a logarithmic law of the wall, which is commonly used for turbulent flows along rough walls. The bubble-equivalent roughness height required by the model was found to correlate very well with the size of the injected gas bubbles. The present work extends this similarity to subcooled boiling flow, where the bubble layer, which is generated by evaporation on the superheated wall, is assumed to act like a rough surface as well. A standard formulation for the logarithmic law of the wall for turbulent flows over rough surfaces is adopted. It is written as

$$u^+ = \frac{1}{\kappa}\ln y^+ + C - \Delta u^+ . \qquad (8)$$

Therein, $u^+ = \bar{u}/u_\tau$ and $y^+ = y u_\tau/\nu$ represent the wall units involving the wall friction velocity $u_\tau = \sqrt{\tau_w/\rho}$ as the relevant velocity scale. C = 5.3 and κ = 0.41 are constants. The last term on the RHS of Eq. (8) represents the offset of u^+ due to the wall roughness with respect to the log law for hydrodynamically smooth surfaces, where $\Delta u^+ = 0$. The offset Δu^+ is a function of the wall-roughness based Reynolds number

$$k_r^+ = \frac{k_r u_\tau}{\nu}, \qquad (9)$$

where k_r is the physical roughness height of the surface. In the specification of the functional dependence $\Delta u^+(k_r^+)$, three different regimes are distinguished (Cebeci & Bradshaw (1977)):

- hydrodynamically smooth, $k_r^+ < 2.25$:

$$\Delta u^+ = 0 \qquad (10)$$

- transitional regime, $2.25 \le k_r^+ < 90$:

$$\Delta u^+ = \frac{1}{\kappa}\ln\left(\frac{k_r^+ - 2.25}{87.75} + C_{kr}\, k_r^+\right)\cdot \sin\left[0.4258\left(\ln k_r^+ - 0.811\right)\right] \qquad (11)$$

- fully rough regime $k_r^+ \ge 90$:

$$\Delta u^+ = \frac{1}{\kappa}\ln\left(1 + C_{kr}\, k_r^+\right). \qquad (12)$$

C_{kr} is a roughness constant and depends on the type of roughness. Its value is set to C_{kr} = 0.5, which corresponds to the value commonly used for sand-grain roughness. In Figure 10 the measured velocity profiles $\bar{u}(y)$ shown in Figures 4a to 7a are recast into the corresponding wall units, and it turns out that the logarithmic law of the wall given by Eq. (8) approximates the data very well in the range $30 < y^+ < 200$. The scaling parameters u_τ and k_r are obtained for each $\bar{u}(y)$-profile from a best fit to the data. The so obtained pairs u_τ and k_r are summarized in Table 1. It is noted that the profiles, which exhibit a plateau in the near-wall region, as shown in Figures 4a and 5a, had to be excluded from this analysis. In these cases, the buoyancy-induced vertical bubble motion is too strong to allow for a simple log-law modeling, which is only applicable if the motion in the wall parallel main flow direction is dominant.

The roughness heights k_r fitted from the experimental data basically represent an equivalent roughness incorporating the dynamic effect of the vapor bubble layer on the liquid flow. This bubble-equivalent roughness height k_r has to be provided by an appropriate model correlation to finally determine the actual near-wall velocity profile using Eq. (8). In the presently proposed correlation, it is assumed that the relevant length scale for the bubble-equivalent roughness height is represented by the bubble diameter d_{dep} at the instant of departure from the nucleation site. This diameter is computed following the bubble detachment model of Zeng *et al.* (1993). In this model, the diameter d_{dep} is obtained from a balance of drag, shear-lift, buoyancy, and bubble-growth forces. As such, the departure diameter is determined as mainly dependent on the wall superheat ΔT_w and the wall friction velocity u_τ. Figure 11 shows the diameters predicted by this detachment model compared to the corresponding experimental data presented in Figure 9. The agreement is very good.

u_b [m/s]	q_w [kW/m²]	u_τ [m/s]	k_r [mm]
0.2	0	0.0131	0
	1.57	0.0147	1.00
	2.62	0.0159	1.71
0.4	0	0.0235	0
	1.56	0.0280	0.49
	2.59	0.0305	0.85
	3.98	0.0326	1.4
	4.73	0.0330	1.85
0.8	0	0.0416	0
	1.56	0.0490	0.23
	2.62	0.0545	0.38
	4.03	0.0593	0.66
	4.65	0.0615	0.85

Table 1: Wall friction velocities and bubble-equivalent roughness heights determined by a least-square fit of the log law to the measured velocity profiles $\overline{u}(y)$ for different bulk velocities and wall heat fluxes. The cases where $q_w = 0$ are single-phase, such that $u_\tau = u_{\tau,1ph}$; all other cases ($q_w > 0$) are two-phase, such that $u_\tau = u_{\tau,2ph}$.

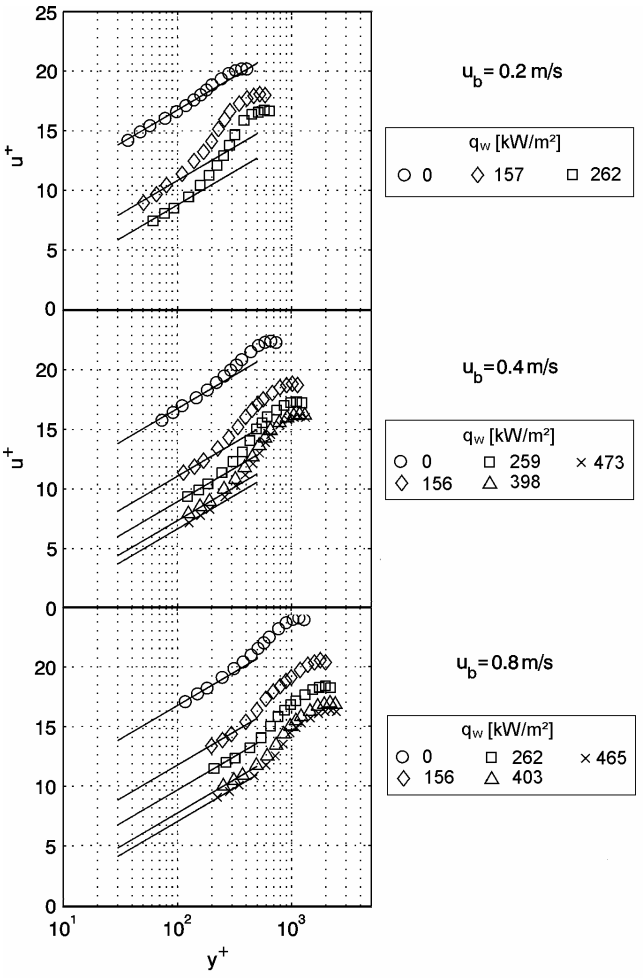

Figure 10: The logarithmic law of the wall (Eq. (8)) compared to the measured velocity profiles in wall units for different bulk velocities u_b and wall heat fluxes q_w. Solid line, "—", log law for rough surfaces.

The so obtained length scale d_{dep} is further modified by the ratio of the nucleate boiling component to the total wall heat flux, q_{nb}/q_w, which represents the boiling activity, and the proposed correlation can be written as

$$\tilde{k}_r = \eta \, d_{dep} \left(\frac{q_{nb}}{q_w} \right)^{\zeta} . \qquad (13)$$

Evidently, as the boiling activity increases, such that q_{nb}/q_w approaches unity, the dynamic influence of the bubble layer on the liquid flow in terms of $\tilde{k}_r$ becomes highest. On the other hand, at very low nucleate boiling heat fluxes q_{nb}, associated with a heater surface sparsely populated with bubbles, the bubble influence on the liquid flow vanishes, and $\tilde{k}_r$ goes to zero.

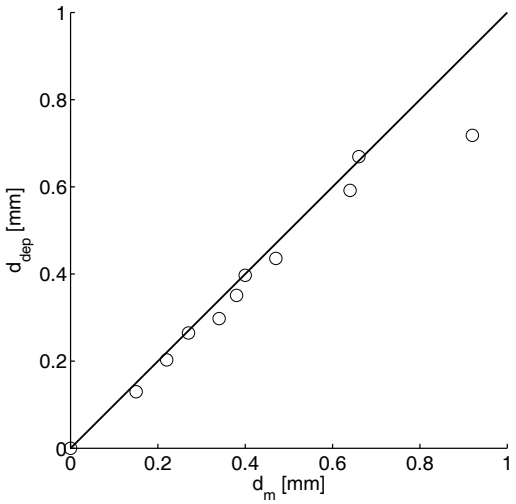

Figure 11: Bubble departure diameters d_{dep} predicted by the model of Zeng *et al.* (1993) in comparison with our experimental data d_m.

The constants η and ζ in Eq. (13) are empirical parameters, which are determined from the experimental data. The determination of the values of these parameters requires the knowledge of q_{nb}, which is very difficult to measure directly. It is therefore obtained indirectly in terms of the convective counterpart. Accordingly, assuming the classical superposition concept for the total wall heat flux q_w introduced by Chen (1963), the nucleate boiling contribution can be written as

$$q_{nb} = q_w - q_{conv,2ph} . \qquad (14)$$

Herein, the convective component $q_{conv,2ph}$ is computed in terms of an enhanced single-phase convection $q_{conv,1ph}$ using the Colburn analogy between the wall heat transfer and the wall friction to describe the enhancement, such that one may write

$$q_{conv,2ph} = q_{conv,1ph} \left(\frac{u_{\tau,2ph}}{u_{\tau,1ph}} \right)^2 . \qquad (15)$$

The ratio $(u_{\tau,2ph}/u_{\tau,1ph})^2$ is determined from the experimental data by relating the measured wall friction velocities for the bubble-laden two-phase cases to those measured in the corresponding bubble-free single-phase cases (see Table 1).

The convective single-phase heat flux $q_{conv,1ph}$ in Eq. (15) is obtained by substituting the experimental $q_w - T_w$ data of the single-phase cases ($T_w < T_{sat}$) into

$$q_{conv,1ph} = \alpha_{conv,1ph}\left(T_w - T_b\right) = q_w \qquad (16)$$

to compute the single-phase heat transfer coefficient $\alpha_{conv,1ph}$ as

$$\alpha_{conv,1ph} = \frac{q_w}{\left(T_w - T_b\right)} \qquad \text{with } T_w < T_{sat}. \qquad (17)$$

Evaluating the proposed model correlation Eq. (13) using those experimental data, where the streamwise motion remains dominant and, hence, the logarithmic law of the wall for rough surfaces is applicable (see Table 1), gives a set of predictions for the bubble-equivalent roughness height $\tilde{k}_r$. In Figure 12 the predicted values for $\tilde{k}_r$ are compared to the corresponding values k_r, which were extracted by best-fit directly from the measured velocity profiles assuming a standard logarithmic law of the wall for rough surfaces (see Figure 10). This fitting procedure revealed that using $\eta = 2.736$ and $\zeta = 0.1665$ leads to the best overall agreement between the modeled bubble-equivalent roughness height $\tilde{k}_r$ and the corresponding values k_r obtained directly from the measured velocity profiles.

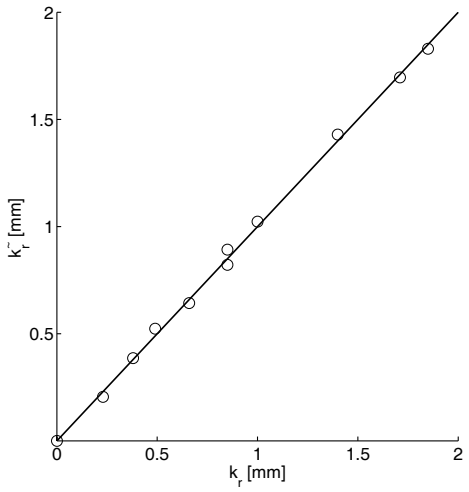

Figure 12: Predicted bubble-equivalent roughness heights $\tilde{k}_r$ in comparison with experimental data.

In the proposed roughness model, the computation of the wall heat flux is coupled with the calculation of the wall shear stress through the modeled bubble-equivalent roughness height $\tilde{k}_r$. This implies a coupled computation of the thermal and the dynamic boundary conditions in an iterative procedure, which is schematically shown in Figure 13. The shown scheme refers to the case of a given bulk velocity u_b and a given wall temperature T_w.

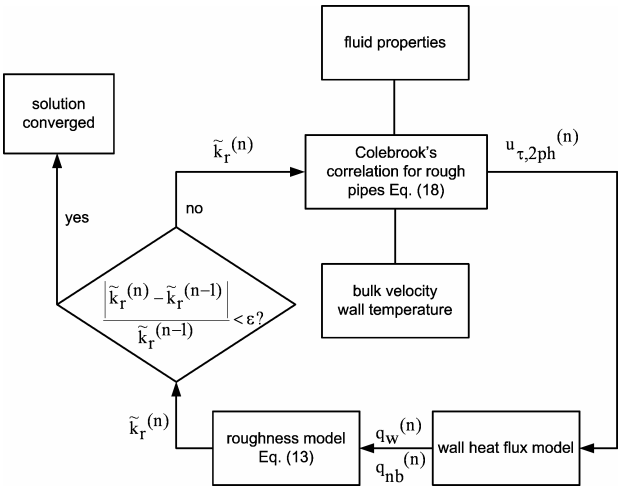

Figure 13: Computational scheme of the roughness model. The superscript (n) denotes the number of each iteration step, and ε is the convergence criterion.

Starting from an initial guess of $\tilde{k}_r = 0$, the bubble-equivalent roughness height, as well as the depending quantities $u_{\tau,2ph}$ and q_w, are recomputed in each loop until the convergence criterion is satisfied. The shear stress velocity $u_{\tau,2ph}$ is related to the given bulk velocity u_b using the well-established correlation for rough pipes according to Colebrook

$$u_{\tau,2ph} = \sqrt{\frac{\lambda_f}{8}}u_b \quad \text{with}$$

$$\lambda_f = \frac{1}{\left[-2\log\left(\frac{2.51}{Re\sqrt{\lambda_S}} + 0.27\,C_{krc}\frac{\tilde{k}_r}{D_h}\right)\right]^2}, \qquad (18)$$

which incorporates the bubble-equivalent roughness height $\tilde{k}_r$. The model parameter C_{krc} basically depends on the topology of the roughness elements. In the present work, this parameter is set to $C_{krc} = 0.65$. In Figure 14 the model predictions for the shear stress velocity $u_{\tau,2ph}$ produced by Eq. (18) using the modeled roughness height $\tilde{k}_r$ are compared to the corresponding values obtained from the measured velocity profiles. The agreement is very good.

The thermal part of the iterative loop sketched in Figure 13 requires the application of an appropriate wall heat flux model. Basically, the ratio q_{nb}/q_w in Eq. (13), which represents the influence of the boiling activity on the bubble-equivalent roughness height $\tilde{k}_r$, suggests the use of a boiling model which explicitly distinguishes between the nucleate boiling and convective contribution to the total wall heat flux. This distinction is inherently met in the framework of the superposition concept.

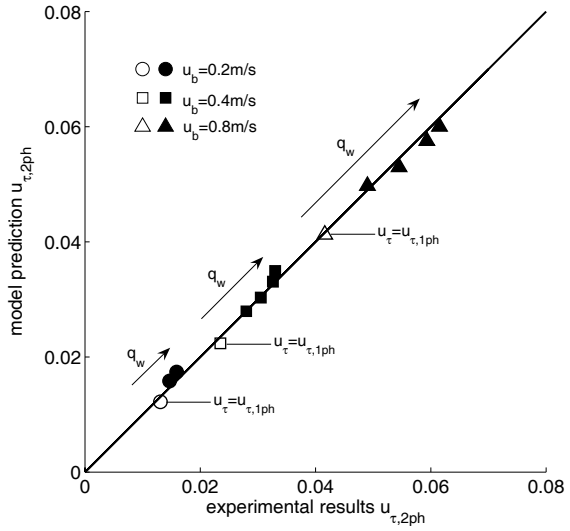

Figure 14: Predicted shear stress velocities $u_{\tau,2ph}$ in comparison with experimental data. The open symbols denote the non-boiling cases. The filled symbols denote the boiling cases.

In the present work, the linear superposition approach introduced by Chen (1963), Eq. (3) is used. When applying Chen's model, the enhancement factor F_{2ph} in Eq. (3) is computed as

$$F_{2ph} = \frac{q_{conv,2ph}}{q_{conv,1ph}} = \left(\frac{u_{\tau,2ph}}{u_{\tau,1ph}} \right)^2 \tag{19}$$

using Colebrook's formula Eq. (18) for $u_{\tau,2ph}$. The single-phase reference value $u_{\tau,1ph}$ is also obtained using Colebrook's formula, but with zero bubble-equivalent roughness height $\tilde{k}_r = 0$. The flow-induced suppression factor is computed following Chen's ansatz

$$S = \frac{1}{1 + a \left(Re\, F_{2ph}^{\,1.25} \right)^b}, \tag{20}$$

which involves the bulk Reynolds number Re and the enhancement factor F_{2ph} as well. The parameters a and b in Eq. (20) are model constants. The nucleate boiling contribution q_{nb} in Eq. (3) is obtained using the well-established pool boiling correlation due to Rohsenow [7]

$$q_{nb} = \left(\frac{c}{h_{fg}} \frac{Pr^{-(\delta+1)}}{C_{sf}} \right)^{1/\gamma} \cdot \cdot \left(\frac{\sigma}{g\,(\rho_l - \rho_v)} \right)^{-1/2} h_{fg}\, \mu_l\, (T_w - T_{sat})^{1/\gamma}, \tag{21}$$

where C_{sf}, δ, and γ are model parameters depending on the combination of surface and fluid. For aqueous solutions, the model parameter δ is usually set to zero, which applies to the present working fluid as well. The model constants were set to $a = 5 \cdot 10^{-6}$, $b = 1.08$, $C_{sf} = 0.0167$, and $\gamma = 0.4$, which provided the best overall agreement of the predicted total wall heat fluxes using Eq. (3) with the experimental results. The predicted boiling curves obtained with the linear superposition, Eq. (3) are shown in Figure 15 in comparison with measurement data represented by symbols. The overall agreement is good.

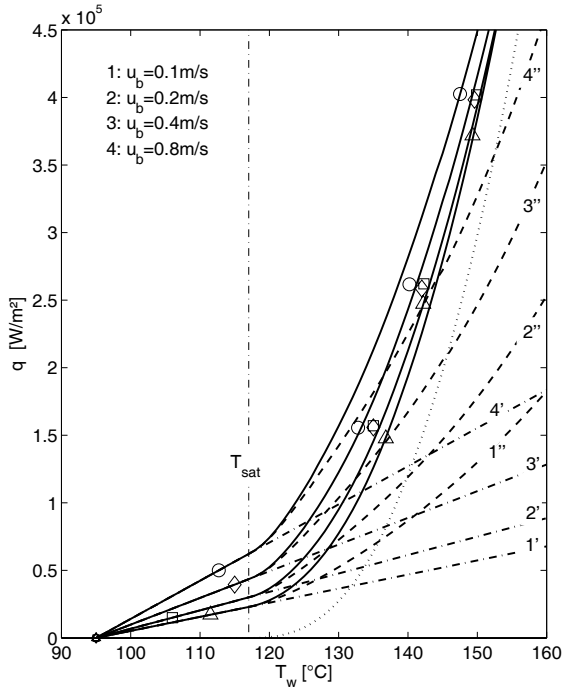

Figure 15: Predicted flow boiling curves using the linear superposition approach according to Eq. (3) at different velocities of the bulk flow: solid line, "——", total wall heat flux q_w; dash-dotted line, "– · – · –", single-phase convective heat flux $q_{conv,1ph}$; dashed line, "– – –", two-phase convective heat flux $q_{conv,2ph}$, dotted line, "· · ·", pool boiling contribution q_{nb} according to Eq. (21); the symbols denote the measurement data.

The asymptotic limits, i.e., the straight single-phase convection lines (dash-dotted lines $1' - 4'$), and the pool boiling curve given by Eq. (21) (dotted line) are also shown in Figure 15. This makes the basic idea behind the superposition approach obvious, which constructs the total wall heat flux q_w as a weighted linear combination of the two asymptotic solutions. The convergence of the individual boiling curves at high wall superheats towards the pool boiling limit is achieved by incorporating a suppression factor S. The enhanced convective contributions $q_{conv,2ph}$ (dashed lines $1'' - 4''$) predicted by the roughness model tend to make up a substantial part of the total wall heat flux q_w, especially for high bulk velocities. The capability of the roughness model to account for the influence of the bubbles on the dynamic boundary condition in terms of an increased shear stress velocity $u_{\tau,2ph}$, as it is demonstrated in Figure 14, has evidently a strong effect on the weight of the superimposed components of the total wall heat flux. The enhanced convective contribution $q_{conv,2ph}$ relative to the corresponding single-phase value $q_{conv,1ph}$ indicates that the present modeling concept can reflect the increased convective heat transfer (bubble-induced micro convection)

associated with the experimentally observed increased turbulence in the bubble-laden wall layer (see Figures 4 and 5). As such the roughness model enables the single-fluid concept to mimic a characteristic feature of the two-phase heat transfer.

Limits of the Proposed Model

The present model presumes the applicability of the standard logarithmic law of the wall used for turbulent near-wall flow over rough surfaces. As seen from Figures 4 and 5, this is clearly not the case for low bulk velocities ($u_b = 0.1$ m/s and $u_b = 0.2$ m/s) at high wall superheats. Under these conditions, a significant plateau is observed in the measured mean velocity profiles in the streamwise direction $\overline{u}(y)$, as shown in Figures 4a and 5a above. This observed plateau excludes any log-law formulation. It can be attributed to the fact that, at low liquid velocities, the bubbles induce a considerable vertical liquid motion, such that the liquid velocity components in the vertical and the streamwise directions assume the same order of magnitude. It was found that the occurrence of such a plateau can be described as mainly dependent on two non-dimensional parameters, the Froude number

$$\mathrm{Fr} = \frac{u_b^2}{g\, d_{dep}} \tag{22}$$

and the Jacob number

$$\mathrm{Ja} = \frac{\rho_l\, c\, (T_w - T_{sat})}{\rho_v\, h_{fg}}\,. \tag{23}$$

The Froude number based on the bulk velocity u_b and the departure diameter d_{dep} of the bubbles represents the ratio of the streamwise to the bubble-driven vertical momentum fluxes, while the Jacob number essentially represents the influence of the wall superheat. The experimental data were non-dimensionalized and introduced into a nomogram of the Froude number versus the Jakob number shown in Figure 16. Some additional cases for bulk velocities $u_b = 0.15$ m/s and $u_b = 0.3$ m/s were introduced as well to provide a broader data base. Data points with the same bulk velocity are connected by dotted lines. The circles denote data points with a plateau in the mean velocity profiles in the streamwise direction. The squares denote those data points without plateau in the velocity profiles, where the logarithmic law of the wall for rough surfaces is applicable. This latter region is termed here the buoyancy-independent regime. A demarcation line (dashed line) which separates the buoyancy-independent from the buoyancy-dependent regime was found empirically and is represented by the equation

$$\mathrm{Fr} = \frac{1}{1 - 0.47\log(\mathrm{Ja})}\,. \tag{24}$$

It becomes very evident that the transition from the buoyancy-independent regime to the buoyancy-dependent regime needs a higher wall superheat (i.e., Jakob number), the higher the bulk velocity is.

It is noted that the limit represented by the demarcation line Eq. (24) is mainly of relevance for the description of the near-wall velocity field, while its relevance for the prediction of the total wall heat flux is comparatively small. As seen from Figure 15, where all cases of the buoyancy-dependent regime are included as well ($u_b = 0.1$ m/s and $u_b = 0.2$ m/s), the corresponding predictions for the total wall heat flux do not exhibit a significant loss in accuracy. This insensitivity to an eventually erroneously predicted microconvective heat transport can be explained by the fact that, in the buoyancy-dependent regime, the total wall heat flux mainly consists of the nucleate boiling contribution to the total wall heat flux and, hence, the convective contribution plays a minor role.

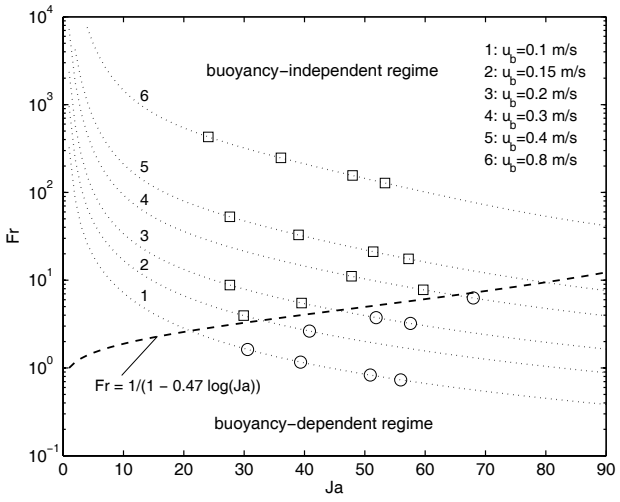

Figure 16: Fr-Ja nomogram for different bulk velocities (dotted lines). The circles ○ denote experimental conditions in the buoyancy-dependent regime; the squares □ denote data from the buoyancy-independent regime. The dashed line is the demarcation curve separating the two regimes found empirically.

Conclusions

Subcooled flow boiling experiments were carried out in a horizontal test channel in order to investigate the near-wall liquid motion under the influence of the vapor bubbles. High-speed camera recordings of the two-phase region were made to gain insight into the size and dynamics of the bubbles. A 2D laser-Doppler anemometer was used to measure the near-wall liquid velocity field. The velocity measurements revealed two main effects of the bubbles. First, the streamwise component is generally decelerated, while the wall-normal component is enhanced. At low liquid Reynolds numbers, the buoyancy-driven motion of the bubbles may become so dominant that a plateau in the mean axial velocity profile is formed. Secondly, it was observed that the turbulent velocity fluctuations are significantly enhanced in the bubble populated region.
Seeking for an appropriate mathematical description of the near-wall streamwise velocity within the framework of single-fluid modeling, it was found that the velocity profiles without plateau follow approximately a log law for turbulent single-phase flow over rough surfaces. Based on these findings, a model was proposed which captures the

influence of the bubbles on the liquid flow in analogy to a surface roughness effect. The proposed model introduces a bubble-equivalent roughness height, which is correlated as dependent on the bubble size and the nucleate boiling contribution to the total wall heat flux. Since the predicted wall shear stress is linked to the wall heat flux through the bubble-equivalent roughness height, the model requires a coupled computation of the dynamic and the thermal boundary conditions in an iterative procedure. Applying Chen's classical linear superposition approach as a submodel for the total wall heat flux gave predictions for the wall friction velocity and the wall heat flux, which are in good agreement with experimental data. An analysis of the individual contributions to the total wall heat flux proved the model capable to reflect the enhanced microconvective momentum and heat transfer caused by the presence of the bubbles in the superheated boundary layer.

At low liquid bulk flow Reynolds numbers, the proposed model reaches its limit, since the near-wall streamwise velocity cannot be represented adequately by a log-law formulation. A non-dimensional criterion for this limitation was specified. Nonetheless, even beyond this limit, the model was proven to produce acceptably accurate predictions for the total wall heat flux. In these cases, the total wall heat flux mainly consists of the nucleate boiling contribution, such that the error introduced by the model into the convective contribution is comparatively small.

Summing up, it can be concluded that, within the framework of a single-fluid modeling, the proposed approach represents a simple, but efficient method to account for the dynamic effect of vapor bubbles on the near-wall liquid flow field, yielding improved dynamic as well as thermal boundary conditions.

Acknowledgements

Financial support of this work from the K plus Competence Center Program initiated by the Austrian Federal Ministry of Transport, Innovation, and Technology (BMVIT) and funded by FFG, Land Steiermark and Steirische Wirtschaftsförderung (SFG) is gratefully acknowledged. We are also grateful for financial support from AVL List GmbH.

References

Campbell, N. A. F., Hawley, J. G., Robinson, K., Joyce, S. & Haigh, M. Predictions for nucleate boiling – results from a thermal bench marking exercise at low flows. SAE Congress, Paper No. 2002-01-1028, Detroit, (2002)

Cebeci, T. & Bradshaw, P. Momentum Transfer in Boundary Layers. Hemisphere, Washington, DC (1977)

Chen, J. C. A correlation for boiling heat transfer to saturated fluids in convective flow. ASME preprint 63 HT34 presented at the 6th National Heat Transfer Conference, Boston (1963)

Cooper, M. G. Nucleate pool boiling using reduced properties. Advances in Heat Transfer, Volume 16, 157–239, (1984)

Forster, H. K. & Zuber, N. Dynamics of vapor bubbles and boiling heat transfer. AIChE J., Volume 1, 531–535 (1955)

Gabillet, C., Colin, C. & Fabre, J. Experimental study of bubble injection in a turbulent boundary layer. International Journal of Multiphase Flow, Volume 28, 553 – 578 (2002)

Gorenflo, D. Behältersieden. VDI Wärmeatlas, Sec. Ha, VDI Verlag Düsseldorf (1988)

Kandlikar, S. G. Heat transfer characteristics in partial boiling, fully developed boiling, and significant void flow regions of subcooled flow boiling. Trans. ASME J. Heat Transfer, Volume 120, 395–401 (1998)

Kutateladze, S. S. Fundamentals of heat transfer. Edward Arnold, London, (1963)

Liu, Z. & Winterton, R. H. S. A general correlation for saturated and subcooled flow boiling in tubes and annuli based on a nucleate boiling equation. Int. J. Heat Mass Transfer Volume 34, 2759–2766 (1991)

Maurus, R. Bestimmung des Blasenverhaltens beim unterkühlten Strömungssieden mit der digitalen Bildfolgenanalyse. PhD thesis, Munich University of Technology (2003)

Mei, R., Klausner, J. F. & Lawrence, C. J. A note on the history force on a spherical bubble at finite Reynolds number. Phys. Fluids, Volume 6, 418–420 (1994)

Mikielewicz, D. Hydrodynamics and heat transfer in bubbly flow in the turbulent boundary layer. Int. J. Heat Mass Transfer, Volume 46, 207–220 (2003)

Rohsenow, W. M. A method of correlating heat transfer data for surface boiling of liquids. Trans. ASME, Volume 74, 969–975 (1952)

Roy, R. P., Velidandla, V. & Kalra, S. P. Velocity Field in Turbulent Subcooled Boiling Flow. ASME J. Heat Transfer, Volume 119, 754–766 (1997)

Roy, R. P., Kang, S., Zarate, J. A. & Laporta, A. Turbulent subcooled boiling flow–experiments and simulations. J. Heat Transfer, Volume 124, 73–93 (2002)

Shah, M. A general correlation for heat transfer during subcooled boiling in pipes and annuli. ASHRAE Trans., Volume 83, Part 1, 205–217 (1977)

Steiner, H., Kobor, A. & Gebhard, L. A wall heat transfer model for subcooled boiling flow. Int. J. Heat Mass Transfer, Volume 48, 4161–4173 (2005)

Steiner, D. & Taborek, J. Flow boiling heat transfer in vertical tubes correlated by an asymptotic model. Heat Transfer Eng., Volume 13, 43–69 (1992)

Troshko, A. A. & Hassan, Y. A. Law of the wall for two-phase turbulent boundary layers. International Journal of Heat and Mass Transfer, Volume 44, 871 – 875 (2001)

Wenzel, U. & Müller-Steinhagen, H. Heat transfer to mixtures of acetone, isopropanol and water under subcooled flow boiling conditions – II. Predictions of heat transfer coefficients. Int. J. Heat Mass Transfer, Volume 33, 185–194 (1994)

Zeng, L. Z., Klausner, J. F., Bernhard, D. M. & Mei, R. A unified model for the prediction of bubble detachment diameters in boiling systems – II. Flow boiling. Int. J. Heat Mass Transfer, Volume 36, 2271–2279 (1993)